Open access • Journal Article • DOI:10.1039/C7TA05877B

In situ TEM observation of the electrochemical lithiation of N-doped anatase TiO2 nanotubes as anodes for lithium-ion batteries — Source link

Minghao Zhang, Minghao Zhang, Kuibo Yin, Kuibo Yin ...+8 more authors

Institutions: University of California, San Diego, Oak Ridge National Laboratory, Southeast University, Georgia Institute of Technology

Published on: 10 Oct 2017 - Journal of Materials Chemistry (The Royal Society of Chemistry)

Topics: Lithium and Anatase

Title

In situ TEM observation of the electrochemical lithiation of N-doped anatase TiO2 nanotubes as anodes for lithium-ion batteries

Journal

JOURNAL OF MATERIALS CHEMISTRY A, 5(39)

ISSN

2050-7488

Authors

Zhang, Minghao
Yin, Kuibo
Hood, Zachary D
et al.

Publication Date

2017-10-21

DOI

10.1039/c7ta05877b

Peer reviewed

Journal of Materials Chemistry A

PAPER

View Article Online
View Journal

Cite this: DOI: 10.1039/c7ta05877b

In situ TEM observation of the electrochemical lithiation of N-doped anatase TiO_2 nanotubes as anodes for lithium-ion batteries†

Minghao Zhang,‡[ae] Kuibo Yin,‡[ac] Zachary D. Hood,‡[ad] Zhonghe Bi,[b] Craig A. Bridges,[b] Sheng Dai,[b] Ying Shirley Meng,[e] Mariappan Parans Paranthaman *[b] and Miaofang Chi *[a]

Received 6th July 2017
Accepted 6th September 2017

DOI: 10.1039/c7ta05877b

rsc.li/materials-a

Due to their high specific capacity and negligible volume expansion during cycling, anatase titanium dioxide (a-TiO_2) nanotubes have been considered as a prime candidate for anodes in lithium-ion batteries. However, their rate capability for electrochemical cycling is limited by the low electronic conductivity of a-TiO_2 nanotubes. Here, we show that a desirable amount of nitrogen doping can significantly enhance the electronic conductivity in a-TiO_2 nanotubes, resulting in improvements in both the capacity stability and the rate capability at fast charge–discharge rates. Electron energy loss spectroscopy revealed a high doping concentration of nitrogen (~5%) by substituting for oxygen ions in a-TiO_2 nanotubes. The lithiation mechanism of N-doped a-TiO_2 nanotubes was further investigated using *in situ* transmission electron microscopy, where a three-step lithiation mechanism was revealed. Lithium ions initially intercalate into the a-TiO_2 lattice structure. Further insertion of lithium ions triggers a phase transformation from a-TiO_2 to orthorhombic $Li_{0.5}TiO_2$ and finally to polycrystalline tetragonal $LiTiO_2$. Our results reveal that nitrogen doping significantly facilitates lithiation in TiO_2 through enhanced electronic conductivity, while the structural and chemical evolutions during the lithiation process remain similar to those of undoped TiO_2.

Introduction

Lithium-ion batteries are one of the most promising energy storage systems for next-generation portable electronic devices and electric vehicles due to their high energy density and power density and long cycle life.[1,2] However, numerous challenges for commercial lithium-ion batteries, such as safety and rate capability, still remain. One of the prime limitations originates from the low discharge potential (below 1 V *vs.* Li^+/Li^0) of carbon-based anodes, which results in electrolyte decomposition and gas evolution during cell cycling. The electrolyte decomposition and gas evolution cause numerous safety problems when batteries overheat.[3,4] Also, the formation of insoluble Li-containing passivating layers on the surface of carbon-based anodes, referred to as the solid electrolyte interphase (SEI) layer, is a major issue during electrochemical cycling of lithium-ion batteries.[3] As a result, industries and researchers continuously search for ideal anode materials for lithium-ion batteries with higher specific capacities, faster kinetics, and superior safety for lithium storage than the currently used graphite anodes.[5–7]

Titanium dioxide (TiO_2) is one of the candidates to replace carbon-based anodes in lithium-ion batteries, thanks to its high specific capacities (around 200–300 mA h g^{-1}) and improved safety performance (high discharge plateau potential around 1.5–1.8 V *versus* lithium) due to the suppression of SEI formation.[8–11] However, electrodes based on TiO_2 suffer from poor electronic conductivity and low Li^+ diffusivity, limiting their rate performance for application in high power appliances. Chemical doping has been previously found as a facile and effective way to improve the rate performance of TiO_2.[12,13] Wang *et al.* have shown that the conductivity of TiO_2 can be enhanced by 2 orders of magnitude by doping with Nb.[12] Tin-doped TiO_2 nanotubes deliver much better rate performance compared to undoped TiO_2 nanotubes. This outstanding rate capability was proposed to be related to the enhanced lithium diffusivity.[13] As such, nitrogen doping is also an effective strategy for improving the rate performance of TiO_2.[14,15] A discharge capacity of 45 mA h g^{-1} has been obtained at the 15C rate for N-doped TiO_2, which was 80% higher than that of pure TiO_2.[14] The electronic

[a]Center of Nanophase Materials Sciences, Oak Ridge National Laboratory, Oak Ridge, Tennessee 37831, USA. E-mail: chim@ornl.gov

[b]Chemical Sciences Division, Oak Ridge National Laboratory, Oak Ridge, Tennessee 37831, USA. E-mail: paranthamanm@ornl.gov

[c]EU-FEI Nano-Pico Center, Southeast University, Nanjing 210096, China

[d]School of Chemistry and Biochemistry, Georgia Institute of Technology, Atlanta, Georgia 30332, USA

[e]Department of NanoEngineering, University of California San Diego (UCSD), La Jolla, CA 92093, USA

† Electronic supplementary information (ESI) available. See DOI: 10.1039/c7ta05877b

‡ These authors contributed equally to the work.

conductivity of TiO_2 was also improved by N doping, which substantially improves the rate capability of TiO_2.[15]

Another strategy to improve the rate performance of TiO_2 is to decrease the particle size through the design of nanostructured materials which can facilitate Li^+ diffusion by shortening the Li^+ insertion/extraction pathway.[16–18] For example, Armstrong *et al.* demonstrated that TiO_2 nanowires possess a better rate capability when compared to bulk TiO_2.[16] Similarly, TiO_2 nanosheets were demonstrated to provide a shorter diffusion distance for Li^+ and are beneficial for the rate performance of the electrode.[17] In particular, TiO_2 nanotubes have been widely explored as anodes for lithium-ion batteries due to the significantly shortened Li^+ diffusion length and an enhanced tolerance to potential volume expansion during cycling.[19,20] TiO_2 nanotubes exhibit excellent high rate performances and their capacity retention at the 10C rate is 74%, compared to that at a rate of 0.5C.[19] TiO_2 nanotube arrays also present good cycling behavior, with capacities between 150 and 230 mA h g^{-1} and a small drop in capacity up to 200 cycles.[20]

Many synthetic methods have been explored to produce TiO_2 nanotubes, namely the chemical template synthesis,[21] the alkaline thermal method,[22] and different electrochemical approaches.[23,24] Electrochemical techniques are some of the most controllable and inexpensive methods to produce TiO_2 nanotube arrays. For instance, we have shown that TiO_2 nanotubes can be synthesized through a technique based on electrochemical anodization, which produced TiO_2 nanotubes with an average length of ~1.5 μm and controllable thicknesses between 80 and 150 nm.[25] These nanotube arrays were demonstrated as effective anodes for lithium-ion batteries. In this work, we integrate both N-doping and a nanotube architecture to demonstrate a further enhanced capacity and stability at fast charge–discharge rates in anatase TiO_2 (a-TiO_2). Various TiO_2 nanotubes ranging from 20 to 100 nm in diameter and up to several micrometers in length were synthesized. In addition, a high concentration of nitrogen doping was successfully achieved by annealing the a-TiO_2 nanotubes under flowing ammonia gas.

Although intense research efforts, including that of both *in situ* spectroscopy and powder X-ray/neutron diffraction on lithium insertion into pristine TiO_2, have been reported,[26,27] the influence of N-doping in a-TiO_2 nanotubes still remains an open question. In particular, the lithiation mechanism, including chemical, structural, and electronic evolutions, has not been well understood for N-doped a-TiO_2 nanotubes. *In situ* methods based on spectroscopy, scanning probe microscopy (SPM), scanning electron microscopy (SEM), neutron diffraction, and X-ray diffraction (XRD) have provided useful information regarding the structural evolution of different electrode materials during the operation of a battery. However, these methods normally have limited spatial resolution. Recently, *in situ* transmission electron microscopy (TEM) techniques have been explored for monitoring different electrochemical reactions of nanostructures in a variety of novel lithium battery electrode materials since *in situ* TEM techniques have superior spatial resolution, which allows for direct observation of dynamic processes occurring in anode materials.[28,29]

Herein, we report our successful design and synthesis of N-doped a-TiO_2 nanotubes and their electrochemical performance in lithium half-cells. Unlike the previous report,[30] the designed N-doped a-TiO_2 exhibits excellent rate performance (discharge capacity is around 100 mA h g^{-1} at 10C rate) without carbon based composites such as graphene nanosheets. Furthermore, *in situ* TEM studies elucidate the electrochemical lithiation mechanism of N-doped TiO_2 nanotubes, and electron energy loss spectroscopy (EELS) was conducted to better ascertain the changes in chemical and electronic properties. This study not only shows that a-TiO_2 nanotubes with a high concentration of substitutional nitrogen exhibit excellent electrochemical performance as an anode material for lithium-ion batteries, but also elucidates the comprehensive structural and phase transformations of TiO_2 upon lithiation of N-doped a-TiO_2 nanotubes.

Experimental

Materials, synthesis of a-TiO_2 nanotubes, and characterization

Titanium foils (99.5%, Alfa Aesar), with a thickness of 0.25 mm, were cut to 1 cm × 5 cm and cleaned for 5 min in deionized water, 5 min in ethanol, and 5 min in acetone by ultrasonication. Then, each substrate was dried under a constant flow of air. A two-electrode electrochemical cell with a platinum cathode was used to anodize Ti foils in an electrolyte solution containing 0.1 M NH_4F (99%, J.T. Baker Inc.), 90 mL of ethylene glycol (99+%, Alfa Aesar), and 10 mL of deionized water. The temperature of the electrolyte solution was maintained at 15 °C using a chiller. The electrochemical anodization of Ti foils was carried out using a Keithley 2612 source meter (Keithley Instruments). Anodized titanium nanotube arrays were post-annealed at 300–350 °C for 30 min while flowing a 4% H_2 in Ar gas mixture followed by annealing at 550 °C for 30 min while flowing ammonia (NH_3) gas to achieve N-doped a-TiO_2 nanotubes. Initial TEM analysis was carried out using a Hitachi HF-3300 TEM/STEM with an energy-dispersive X-ray spectrometer at 300 kV to confirm the sample homogeneity and morphology.

Electrochemical performance

Two-electrode electrochemical test cells were assembled in an Ar-filled glovebox using a-TiO_2 nanotubes on titanium foil as the working electrode and metallic lithium foil as the counter/reference electrode. The nanotubes on the opposite side of the titanium foil were removed to ensure good contact between the electrode and the current collector. All electrochemical tests were conducted with an electrolyte solution consisting of 1 M $LiPF_6$ in ethylene carbonate (EC)/dimethyl carbonate (DMC) (1 : 1 by volume) without the use of binders or conductive carbon. The active mass of the nanotubes was estimated by collecting the a-TiO_2 from one side of the titanium foil and assuming a symmetric mass distribution during the synthesis of a-TiO_2. Battery cells consisting of a-TiO_2 were charged/discharged galvanostatically at room temperature under different rates at potentials ranging between 1 V and 2.5 V using an Arbin Instruments potentiostat/galvanostat multichannel

system. Impedance spectra were recorded in the frequency range 10^5–0.1 Hz with a signal amplitude of 10 mV using a VersaSTAT 4 Potentiostat (Princeton Applied Research) attached to an internal frequency response analyzer.

In situ TEM setup

In situ TEM characterization was carried out on an aberration-corrected FEI Titan 80/300 microscope equipped with a Gatan Quantum ER EELS spectrometer. EELS spectra were acquired with a collection semi-angle of 50 mrad, and each spectrum presented in this paper is the sum of 40 spectra. For the case of the present work, to minimize the effect of the electron beam on the sample, the beam was blocked during the charging process. During the imaging, the electron dose to the a-TiO_2 nanotubes was minimized by spreading the electron beam over large areas. Therefore, the electron beam modification of the general microstructure presented in the paper is at a minimum.

All *in situ* TEM experiments utilized a specialized holder (Nanofactory Instruments) that allowed for the creation of a nanoscale electrochemical cell inside the TEM.[31] The holder features two metallic probes that can be moved *via* piezo control. One side of the electrochemical cell consists of a tungsten probe where lithium metal is dispersed on the tip. The lithium metal is coated with a thin layer of lithium oxide after being intentionally exposed to air for several seconds. The other side of the TEM holder contains a gold probe, where a copper grid with a collection of N-doped a-TiO_2 nanotubes was attached. To begin the *in situ* TEM experiment, the lithium metal electrode was positioned so that it came into contact with the a-TiO_2 nanotubes. The oxide layer on the surface of the lithium metal prevents direct chemical reactions and acts as a solid electrolyte layer through which lithium ions can pass. The TiO_2 electrode was set at 2.5 V *versus* the lithium electrode to simulate true electrochemical processes in an electrochemical cell that include a-TiO_2 nanotubes at the anode. The applied overpotential is larger than the electrochemical window (1–2 V) of a conventional TiO_2–Li half-cell, which enables Li^+ diffusion through the Li_2O layer. Once Li^+ ions reach the a-TiO_2 nanotubes, the electrochemical reaction does not directly depend on the battery setup. In other words, the voltage applied to the nanotubes in this setup equals the applied potential (2.5 V) minus the potential drop in the Li_2O electrolyte and the IR drop due to contact resistance. This makes the lithiation behavior observed in this work comparable to the macroscopic performance of the battery.

Results and discussion

Fig. 1a shows a representative TEM image of N-doped a-TiO_2 nanotubes. As shown in this image, nitrogen doping appears to have little effect on the morphology of a-TiO_2 nanotubes. The N-doped a-TiO_2 nanotubes have a typical inner diameter of about 80–90 nm with a wall thickness of about 20 nm and were up to several micrometers in length. Furthermore, EELS reveals uniform N-doping throughout the a-TiO_2 nanotubes. Fig. 1b shows a typical nitrogen K-edge of a-TiO_2 nanotubes after nitrogen doping. The concentration of nitrogen in a-TiO_2 was further quantified to be ~7 atomic % by comparing the edge integrations of the nitrogen K-edge and the titanium L-edge, representing the highest reported nitrogen content for N-doped TiO_2. Furthermore, the change in oxygen content of the N-doped nanotubes was estimated by using EELS quantification to compare the elemental ratios in N-doped and undoped TiO_2 samples, as shown in Fig. S1.† It was revealed that the oxygen content decreased by around 10 atomic % after nitrogen doping, indicating partial substitution of oxygen with nitrogen.

The typical charge/discharge curves of the a-TiO_2 nanotubes with and without nitrogen doping are shown in Fig. 2a. The capacity increased from 150 to 200 mA h g^{-1} (corresponding to an increase of 0.15 moles of Li during lithiation per mole of TiO_2) after nitrogen doping at the same charge/discharge rate (0.1C). To further investigate the electrochemical properties of the pure and N-doped a-TiO_2 nanotube electrodes, the rate capability was tested for each of these materials (Fig. 2b). It can be seen that the capacity of the pure a-TiO_2 nanotubes decreased from 150 to 25 mA h g^{-1} when the charge/discharge rate increased from 0.1C to 10C. For N-doped a-TiO_2 nanotubes, the capacity only decreased from 200 mA h g^{-1} to 100 mA h g^{-1} under the same conditions. The anatase structure of pure TiO_2 is maintained in the nitrogen-doped nanotubes due to the low doping levels. Overall, the electrochemical performance of N-doped a-TiO_2 nanotubes has been significantly improved when compared with that of pure a-TiO_2 tubes. The enhanced

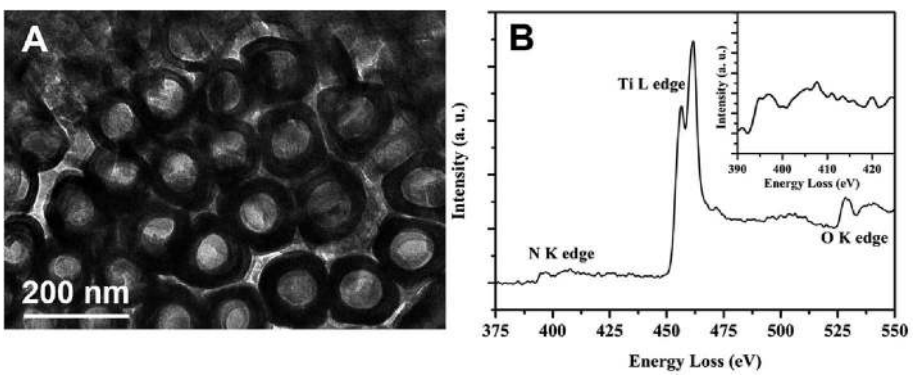

Fig. 1 (A) TEM image of N-doped a-TiO_2 nanotubes. (B) EELS spectrum of N-doped a-TiO_2 nanotubes with the nitrogen K-edge as the inset.

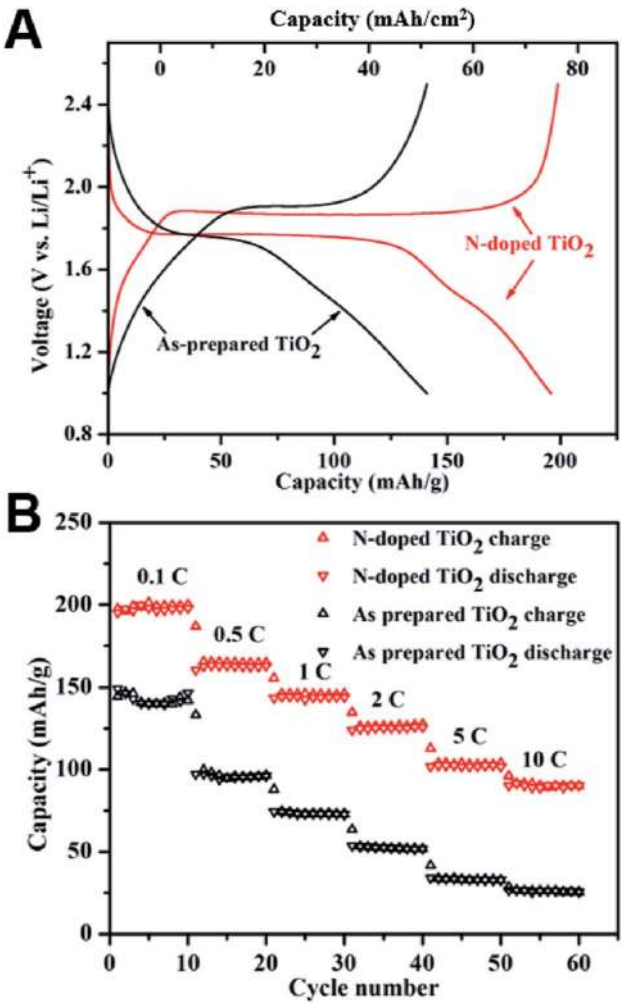

Fig. 2 (A) Room temperature charge/discharge curves at C/10 for a-TiO_2 nanotubes with and without nitrogen-doping. (B) Cycling and rate performance of a-TiO_2 nanotubes with and without nitrogen-doping. All electrochemical measurements were completed in a coin cell configuration.

charge/discharge properties in N-doped a-TiO_2 nanotubes are related to the electronic properties due to nitrogen doping. To understand the effects of nitrogen doping on the electronic properties, electrochemical impedance spectra were recorded for pure a-TiO_2 nanotube and N-doped a-TiO_2 nanotube electrodes. Fig. S2† shows the Nyquist plots of TiO_2 nanotube arrays at the open-circuit potential as well as the corresponding equivalent circuit to fit the plots. R_s is the electrolyte resistance while R_{sei} and R_{ct} correspond to the resistances of the solid electrolyte interface (SEI) and the charge transfer resistance, respectively. The R_s, R_{sei} and R_{ct} values for pure a-TiO_2 nanotubes are 21.9, 3.7 and 45.4 Ω cm^2, respectively. The ohmic resistances of R_s, R_{sei} and R_{ct} decrease to 8.4, 3.2, and 36.3 Ω cm^2 for N-doped a-TiO_2 nanotubes, respectively. It should be noted that no additives such as binders or carbon black were used in the fabrication of the coin cells for battery testing, which indicates that the total ohmic resistance of the coin cell is determined by the conductivity of the nanotube layers. This result shows that nitrogen doping is an effective way to improve the electrical conductivity of a-TiO_2. Oxygen vacancies are introduced into a-TiO_2 nanotubes due to nitrogen doping to maintain charge neutrality. Oxygen defects or vacancies can act as electron acceptors in the material, which can also be responsible for the observed improvement in electrical conductivity.[32]

In situ TEM was then applied to further understand the detailed morphological changes and structural transformations upon lithiation in N-doped a-TiO_2 nanotubes. Fig. 3a and b show the bright-field TEM images of an individual N-doped a-TiO_2 nanotube before and after complete lithiation, respectively. The pristine N-doped a-TiO_2 nanotubes have an inner diameter of about 85 nm and the wall thickness of the marked nanotube is about 21 nm. After lithiation, the inner diameter of the tube increased to 89 nm and the thickness of the wall increased to 23 nm, which corresponds to ~6% expansion in the radial direction after lithiation of the a-TiO_2 nanotube. In the previous *in situ* TEM study of pure TiO_2 nanotubes, the inner diameter of the nanotube remained unchanged (see Fig. S3†) because of the limited electronic conductivity of pure TiO_2 without nitrogen doping.[33] Furthermore, an overpotential as high as 4 V was applied to initiate the lithiation process in the previous work. All of these phenomena may be a consequence of the different electrical conductivities in doped and undoped TiO_2 nanotubes. Although it is difficult to directly measure the elongation of each nanotube with the current *in situ* setup, the overall volume expansion for the N-doped a-TiO_2 nanotube can be estimated based on the geometry. The overall volume expansion is dependent on the ratios of S_f/S_i and l_f/l_i, where S is the area of the circular base of the tube and l is the length of the tube. In Fig. 3, the ratio of S_f/S_i of the nanotube is only 0.0036. Therefore, the overall volume expansion for the a-TiO_2 tube is within 3%, which is consistent with recent *ex situ* studies.[34,35]

HRTEM images of the a-TiO_2 nanotubes before and after lithiation are displayed in Fig. 3c and d. The pristine N-doped TiO_2 nanotube has a pure anatase phase. After lithiation, a thin layer is formed on the outside surface of the a-TiO_2 nanotube measuring about 10 nm, which is marked by the black dashed lines. A close examination of the lithiated a-TiO_2 nanotubes indicates that the surface layer is composed of polycrystalline Li_2O. The upper left inset of Fig. 3d shows the FFT from the surface region with (111) and (220) indexed planes, which correspond to the Li_2O phase. In our studies, we did not see clear evidence of the formation of the Li_2O layer inside the nanotube. This result is not difficult to understand: the formation of this Li_2O layer is likely attributed to lithium ions reacting with residual oxidic groups on the surface of the a-TiO_2 nanotubes.[36] During *in situ* TEM experiments, the solid electrolyte is the component that directly contacts with nanotube outer surface only. The chance for the inner surface to create a layer of oxide requests the Li ions to travel to the inner surface under certain local potentials. Once Li ions diffuse throughout the outside surface of the nanotubes, intercalation reactions occur, resulting in a smaller accumulation of free Li ions on the inner surface of the nanotubes. In comparison, the formation of an oxide layer on the outer surface is much easier because (1) the direct contact between the N-doped TiO_2 outer surface and solid electrolyte lowers surface layer

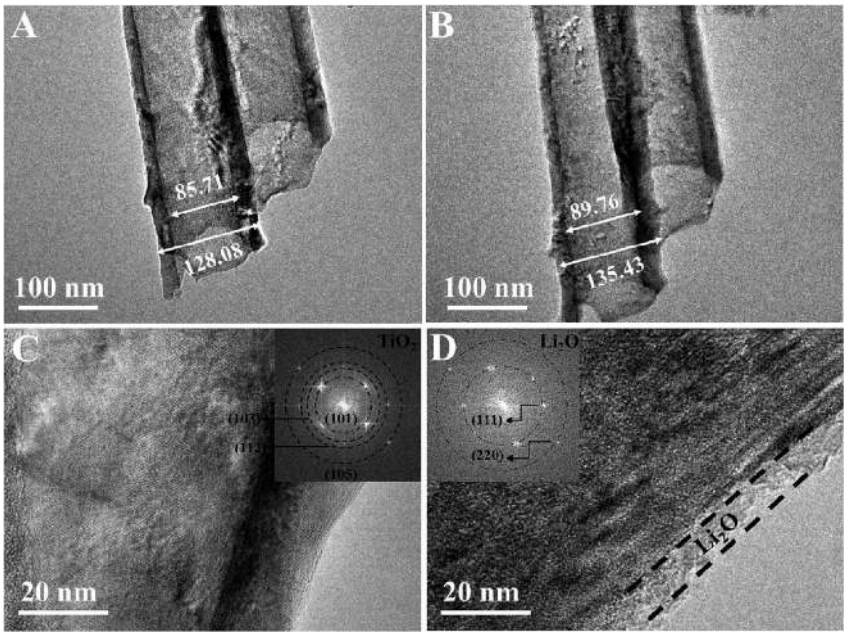

Fig. 3 Bright-field TEM images of an individual N-doped a-TiO_2 nanotube (A) before lithiation and (B) after complete lithiation displaying clear volume expansion. HRTEM images of an individual N-doped TiO_2 nanotube (C) before lithiation and (D) after lithiation showing the formation of a Li_2O layer. The insets are the corresponding FFT patterns from the a-TiO_2 nanotube surface region.

formation potential, and (2) a partial Li_2O layer on the Li metal tip can potentially migrate to the outer surface of the nanotubes. Therefore, we believe that the formation of a Li_2O layer on the inner surface of the nanotubes is limited.

To further reveal transformations in the N-doped anatase TiO_2 microstructure during lithiation, *in situ* TEM images of an individual a-TiO_2 nanotube were collected at different time points during the lithiation process (Fig. 4). The inset of Fig. 4a shows the FFT from the bulk region where the pattern can be indexed to a mixture of anatase TiO_2 ($I4_1/amd$) and orthorhombic $Li_{0.5}TiO_2$ (*Imma*). This observation illustrates the first phase transition where anatase TiO_2 and orthorhombic $Li_{0.5}TiO_2$ coexist. This observation also demonstrates the possibility of Li^+ intercalation into a-TiO_2 at the very beginning of the lithiation process. The presence of $Li_{0.5}TiO_2$ occurs at the main plateau around 1.75 V in the typical charge/discharge curve. The original a-TiO_2 phase

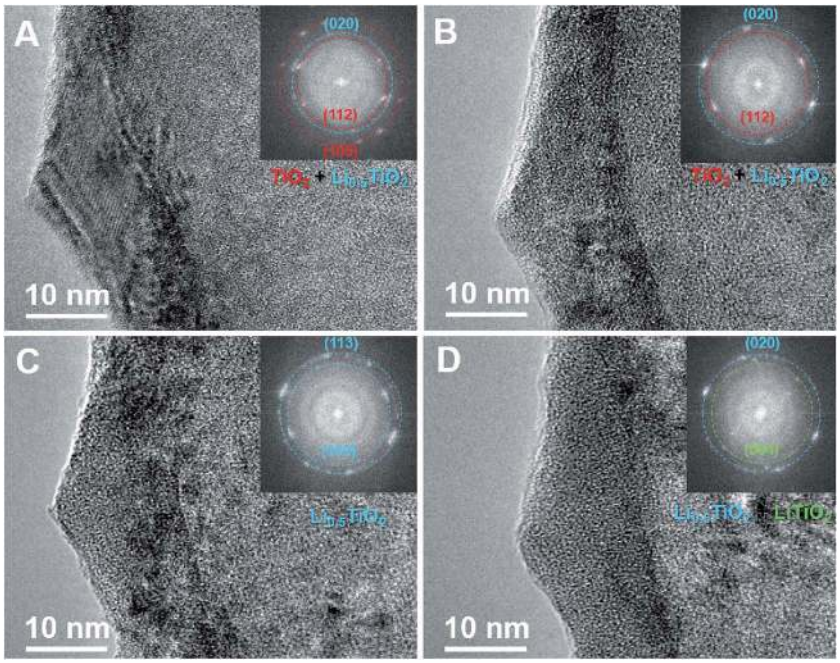

Fig. 4 (A–D) TEM images taken during *in situ* lithiation of an individual N-doped TiO_2 nanotube. The insets correspond to FFT patterns from the bulk region of the a-TiO_2 nanotube.

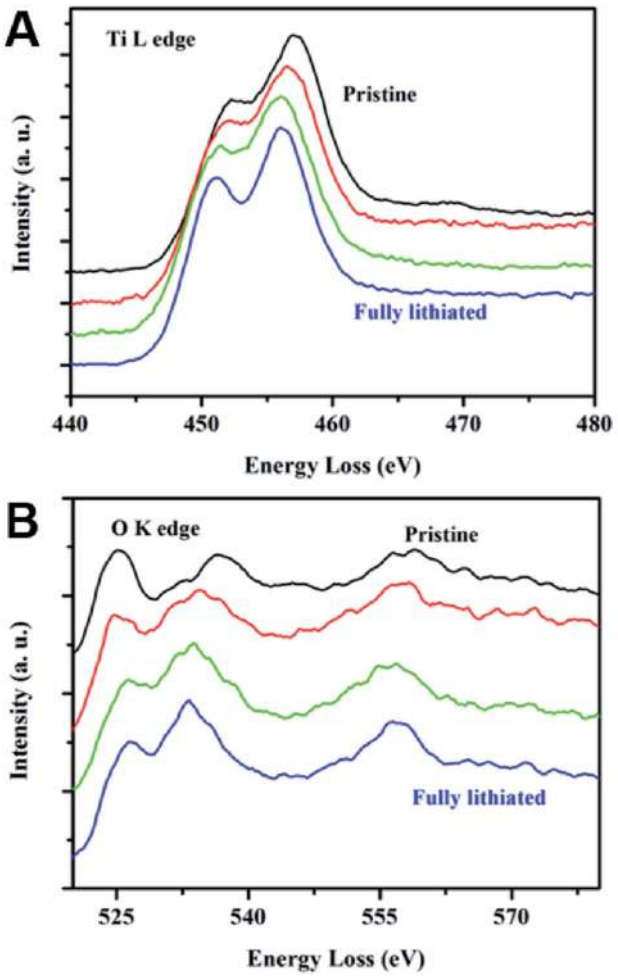

Fig. 5 (A) Titanium L-edge and (B) oxygen K-edge of N-doped a-TiO_2 nanotubes at different stages during the lithiation process.

gradually transforms to the orthorhombic $Li_{0.5}TiO_2$ phase until all of the material becomes $Li_{0.5}TiO_2$ (Fig. 4b and c) towards the end of the constant voltage plateau. After this first transition, lithium is further inserted into $Li_{0.5}TiO_2$, causing the structure to evolve from orthorhombic $Li_{0.5}TiO_2$ to tetragonal $LiTiO_2$ ($I4_1/amd$) as shown in Fig. 4d. This second transition corresponds to the dip in the charge/discharge curve at around 1.4 V *versus* Li/Li^+. Compared with the pristine a-TiO_2, the $LiTiO_2$ phase is polycrystalline with Li^+ fully occupying the octahedral sites. Due to the better electrical conductivity of N-doped TiO_2 nanotubes, Li ions can intercalate deep into the interior structure of the nanotubes, which makes the lithiation process more complete. As a result, all three phases, including anatase TiO_2 ($I4_1/amd$), orthorhombic $Li_{0.5}TiO_2$ (*Imma*), and tetragonal $LiTiO_2$ ($I4_1/amd$), were well captured in our study. These two phase transitions are also consistent with a previous study by Lafont *et al.*[26] In their work, TiO_2 nanoparticles were used to investigate the lithiation mechanism through *in situ* XRD and XAS. Additionally, different TiO_2 microstructures, such as nanowires and nanosheets, were also demonstrated to be beneficial for the rate performance of the TiO_2 electrode with a similar lithiation process observed in our study.[16,17]

EELS was conducted on the N-doped a-TiO_2 nanotube at different lithiation steps to investigate chemical changes during lithiation. Fig. 5a shows the EELS of the titanium L-edge in the nanotube before and after lithiation. The main feature of the titanium L-edge is splitting into $2p_{3/2}$ and $2p_{1/2}$ levels, which is a result of the transition from $2p_{3/2}$ to $3d_{3/2}$ and $3d_{5/2}$ and from $2p_{1/2}$ to $3d_{3/2}$, respectively. The energy loss position of this peak is sensitive to the valence of titanium. After lithiation, the positions of these two energy levels shift to a lower energy region, indicating that the valence of Ti^{4+} reduces to Ti^{3+}, which is consistent with the observation of the structural transformations from the original a-TiO_2 phase to the tetragonal $LiTiO_2$ phase in Fig. 4. It should be noted that not all Ti^{4+} cations are reduced to Ti^{3+} and some orthorhombic $Li_{0.5}TiO_2$ phase still exists in the fully lithiated state of the N-doped a-TiO_2 nanotube based on the observations in Fig. 4d.

Additional evidence of the chemical changes in a-TiO_2 is provided by the oxygen K-edge spectra obtained at different time points during *in situ* lithiation (Fig. 5b). The oxygen K-edge is due to the transition of 1s electrons to the unoccupied 2p orbitals, which are hybridized with titanium 3d orbitals. The splitting of the oxygen K-edge corresponds to the splitting of titanium 3d orbitals (t_{2g} orbitals at a lower energy level and e_g orbitals at a higher energy level) due to the crystal field of the a-TiO_2 structure. After lithiation, the ratio of the first peak to the second peak decreases, which may result from a smaller number of unoccupied t_{2g} orbitals in the neighboring titanium ions. The increasing amount of electrons in t_{2g} orbitals results in the reduction of Ti^{4+} to Ti^{3+}. Another notable feature in the oxygen K-edge spectra during lithiation is the decrease in separation between the two peaks. Previous studies have shown that the separation between the two peaks on the oxygen K-edges is highly dependent on the valence change in the titanium ions.[37] The observed decrease in the separation between these two peaks indicates the valence reduction of titanium to accommodate Li^+ intercalation. These EELS results are therefore in good agreement with the intercalation mechanism of Li^+ into N-doped a-TiO_2 revealed by our HRTEM and FFT analysis (Fig. 4).

Conclusions

N-doped a-TiO_2 nanotubes have overall improved electrochemical performance compared to bulk TiO_2 when employed as an anode material for lithium-ion batteries. When the charge–discharge rate increased from 0.1C to 10C, the capacity only decreased from 200 to 100 mA h g^{-1} for N-doped a-TiO_2 nanotubes. This dramatic improvement is attributed to the optimization of the material in terms of both the structure and the morphology, which can advance the commercial use of TiO_2 anode materials. *In situ* TEM combined with EELS reveals detailed morphological changes and phase transformations during the lithiation process for N-doped a-TiO_2 nanotubes. The pristine a-TiO_2 phase undergoes two phase transitions upon lithiation: anatase TiO_2 ($I4_1/amd$) to orthorhombic $Li_{0.5}TiO_2$ (*Imma*) and then $Li_{0.5}TiO_2$ (*Imma*) to tetragonal $LiTiO_2$ ($I4_1/amd$). These *in situ* TEM observations reveal that morphological changes and phase transformations allow for a-TiO_2 nanotube

anodes to have overall enhanced electrochemical performance in lithium-ion batteries.

Conflicts of interest

There are no conflicts to declare.

Acknowledgements

This research was sponsored by the Center for Nanophase Materials Sciences (CNMS), which is a DOE Office of Science User Facility (MZ, MC), and by the U.S. Department of Energy, Office of Science, Basic Energy Sciences, Materials Sciences and Engineering Division (ZB, CAB, SD, MPP, MC). ZDH acknowledges a Graduate Research Fellowship from the National Science Foundation (No. DGE-1650044) and the Georgia Tech-ORNL Fellowship. KY acknowledges the support from the Natural Science Foundation of China and Jiangsu Province (No. 11674052 and BK2012123). Note: this manuscript has been authored by UT-Battelle, LLC under Contract No. DEAC05-00OR22725 with the U.S. Department of Energy. The United States Government retains and the publisher, by accepting the article for publication, acknowledges that the United States Government retains a non-exclusive, paid-up, irrevocable, world-wide license to publish or reproduce the published form of this manuscript, or allow others to do so, for United States Government purposes. The Department of Energy will provide public access to these results of federally sponsored research in accordance with the DOE Public Access Plan (http://energy.gov/downloads/doe-public-access-plan).

References

1 M. Armand and J.-M. Tarascon, *Nature*, 2008, **451**, 652–657.
2 J.-M. Tarascon and M. Armand, *Nature*, 2001, **414**, 359–367.
3 S.-E. Lee, E. Kim and J. Cho, *Electrochem. Solid-State Lett.*, 2007, **10**, A1–A4.
4 P. Poizot, S. Laruelle, S. Grugeon, L. Dupont and J. Tarascon, *Nature*, 2000, **407**, 496–499.
5 R. Gitzendanner, F. Puglia, C. Martin, D. Carmenn, E. Jones and S. Eaves, *J. Power Sources*, 2004, **136**, 416–418.
6 Y. Shao-Horn, L. Croguennec, C. Delmas, E. C. Nelson and M. A. O'Keefe, *Nat. Mater.*, 2003, **2**, 464–467.
7 B. Kang and G. Ceder, *Nature*, 2009, **458**, 190–193.
8 A. R. Armstrong, C. Arrouvel, V. Gentili, S. C. Parker, M. Saiful Islam and P. G. Bruce, *Chem. Mater.*, 2010, **22**, 6426–6432.
9 G. Armstrong, A. R. Armstrong, J. Canales and P. G. Bruce, *Chem. Commun.*, 2005, 2454–2456.
10 D. V. Bavykin and F. C. Walsh, *Titanate, Titania Nanotubes*, The Royal Society of Chemistry, Cambridge, U.K., 2010.
11 W. J. H. Borghols, M. Wagemaker, U. Lafont, E. M. Kelder and F. M. J. Mulder, *J. Am. Chem. Soc.*, 2009, **131**, 17786–17792.
12 Y. Wang, B. M. Smarsly and I. Djerdj, *Chem. Mater.*, 2010, **22**, 6624–6631.
13 N. A. Kyerematenga, F. Vacandio, M.-T. Sougrati, H. Martinezd, J.-C. Jumasc, P. Knauthb and T. Djenizian, *J. Power Sources*, 2013, **224**, 269–277.
14 Y. Q. Zhang, F. Du, X. Yan, Y. M. Jin, K. Zhu, X. Wang, H. M. Li, G. Chen, C. Z. Wang and Y. J. Wei, *ACS Appl. Mater. Interfaces*, 2014, **6**, 4458–4465.
15 S. Yoon, C. A. Bridges, R. R. Unocic and M. P. Paranthaman, *J. Mater. Sci.*, 2013, **48**, 5125–5131.
16 A. R. Armstrong, G. Armstrong, J. Canales and P. G. Bruce, *Angew. Chem., Int. Ed.*, 2004, **43**, 2286–2288.
17 F. Wu, Z. Wang, X. Li and H. Guo, *Ceram. Int.*, 2014, **40**, 16805–16810.
18 G. Zhang, H. B. Wu, T. Song, U. Paik and X. W. Lou, *Angew. Chem., Int. Ed.*, 2014, **53**, 12590–12593.
19 J. Kim and J. Cho, *J. Electrochem. Soc.*, 2007, **154**(6), A542–A546.
20 Q. L. Wu, J. C. Li, R. D. Deshpande, N. Subramanian, S. E. Rankin, F. Q. Yang and Y. T. Cheng, *J. Phys. Chem. C*, 2012, **116**, 18669–18677.
21 J. C. Hulteen and C. R. Martin, *J. Mater. Chem.*, 1997, **7**(7), 1075–1087.
22 T. Kasuga, M. Hiramatsu, A. Hoson, T. Sekino and K. Niihara, *Langmuir*, 1998, **14**(12), 3160–3163.
23 D. Gong, C. A. Grimes, O. K. Varghese, W. C. Hu, R. S. Singh, Z. Chen and E. C. Dickey, *J. Mater. Res.*, 2001, **16**, 3331–3334.
24 L. V. Taveiraa, J. M. Macákb, H. Tsuchiyab, L. F. P. Dicka and P. Schmuki, *J. Electrochem. Soc.*, 2005, **152**(10), B405–B410.
25 Z. H. Bi, M. P. Paranthaman, P. A. Menchhofer, R. R. Dehoff, C. A. Bridges, M. F. Chi, B. K. Guo, X. G. Sun and S. Dai, *J. Power Sources*, 2013, **222**, 461–466.
26 U. Lafont, D. Carta, G. Mountjoy, A. V. Chadwick and E. M. Kelder, *J. Phys. Chem. C*, 2010, **114**, 1372–1378.
27 V. Gentili, S. Brutti, L. J. Hardwick, A. R. Armstrong, S. Panero and P. G. Bruce, *Chem. Mater.*, 2012, **24**, 4468–4476.
28 D. Qian, C. Ma, K. L. More, Y. S. Meng and M. Chi, *NPG Asia Mater.*, 2015, **7**, e193.
29 K. Yin, M. Zhang, Z. D. Hood, J. Pan, Y. S. Meng and M. Chi, *Acc. Chem. Res.*, 2017, **50**(7), 1513–1520.
30 Y. Li, Z. Wang and X. J. Lv, *J. Mater. Chem. A*, 2014, **2**, 15473–15479.
31 C. Ma, Y. Cheng, K. Yin, J. Luo, A. Sharafi, J. Sakamoto, J. Li, K. L. More, N. J. Dudney and M. Chi, *Nano Lett.*, 2016, **16**, 7030–7036.
32 A. Kalabukhov, R. Gunnarsson, J. Borjesson, E. Olsson, T. Claeson and D. Winkler, *Phys. Rev. B: Condens. Matter Mater. Phys.*, 2007, **75**, 121404.
33 Q. Gao, M. Gu, A. Nie, F. Mashayek, C. Wang, G. M. Odegard and R. Shahbazian-Yassar, *Chem. Mater.*, 2014, **26**, 1660–1669.
34 D. Guan, C. Cai and Y. J. Wang, *J. Nanosci. Nanotechnol.*, 2011, **11**, 3641–3650.
35 Z. Wei, Z. Liu, R. Jiang, C. Bian, T. Huang and A. J. Yu, *J. Solid State Electrochem.*, 2010, **14**, 1045–1050.
36 Q. Su, L. Chang, J. Zhang, G. Du and B. J. Xu, *J. Phys. Chem. C*, 2013, **117**, 4292–4298.
37 M. Yoshiya, I. Tanaka, K. Kaneko and H. J. Adachi, *J. Phys.: Condens. Matter*, 1999, **11**, 3217–3228.